A Note on Soil Moisture Memory and Interactions with Surface Climate for Different Vegetation Types in the La Plata Basin

ANNA A. SÖRENSSON

Centro de Investigaciones del Mar y la Atmósfera, Consejo Nacional de Investigaciones Científicas y Técnicas–Universidad de Buenos Aires, UMI IFAECI/CNRS, Buenos Aires, Argentina

ERNESTO HUGO BERBERY

Cooperative Institute for Climate and Satellites–Maryland, Earth System Science Interdisciplinary Center, University of Maryland, College Park, College Park, Maryland

(Manuscript received 30 May 2014, in final form 4 December 2014)

ABSTRACT

This work examines the evolution of soil moisture initialization biases and their effects on seasonal forecasts depending on the season and vegetation type for a regional model over the La Plata basin in South America. WRF–Noah simulations covering multiple cases during a 2-yr period are designed to emphasize the conceptual nature of the simulations at the expense of the statistical significance of the results. Analysis of the surface climate shows that the seasonal predictive skill is higher when the model is initialized during the wet season and the initial soil moisture differences are small. Large soil moisture biases introduce large surface temperature biases, particularly for savanna, grassland, and cropland vegetation covers at any time of the year, thus introducing uncertainty in the surface climate. Regions with evergreen broadleaf forest have roots that extend to the deep layer whose moisture content affects the surface temperature through changes in the partitioning of the surface fluxes. The uncertainties of monthly maximum temperature can reach several degrees Celsius during the dry season in cases when 1) the soil is much wetter in the reanalysis than in the WRF–Noah equilibrium soil moisture and 2) the memory of the initial value is long because of scarce rainfall and low temperatures. This study suggests that responses of the atmosphere to soil moisture initialization depend on how the initial wet and dry conditions are defined, stressing the need to take into account the characteristics of a particular region and season when defining soil moisture initialization experiments.

1. Introduction

Current attempts at producing seasonal forecasts rely primarily on the influence of large-scale modes of ocean variability and persistent atmospheric patterns. Much of the effort involves the development of models that can represent the ocean–atmosphere coupling with enough skill to produce seasonal forecasts. In recent years, studies have shown that land surface processes can contribute to improving the seasonal predictive skill of models in regions of strong land–atmosphere interaction and soil moisture memory (Dirmeyer 2000; Koster et al. 2010).

Soil moisture affects the atmosphere through evapotranspiration, which is the link between the water and energy budgets. Therefore, the sensitivity of evapotranspiration to soil moisture is a necessary condition for soil moisture to act as a predictor of the surface climate. A model's predictive skill due to surface processes is commonly presented in the context of the soil moisture–atmosphere coupling and soil moisture memory. The coupling concept refers to the influence of soil moisture on any atmospheric variable such as precipitation, evapotranspiration, or surface temperature. This notion emerges from a need to isolate the direction of causality between the two variables, since precipitation in most cases exerts a strong control on soil moisture. The influence of soil moisture on the atmosphere is a result of complex and nonlinear interactions between multiple processes within the climate system (Koster et al. 2004, 2006). The soil moisture memory is a measure of the

Corresponding author address: Anna A. Sörensson, CIMA (CONICET-UBA), Piso 2, Pabellón 2, Ciudad Universitaria, Int. Guiraldes 2160, C1428EGA Buenos Aires, Argentina.
E-mail: sorensson@cima.fcen.uba.ar

DOI: 10.1175/JHM-D-14-0102.1

time length that a moisture anomaly is detectable and during which it can influence the atmosphere. Coupling and memory concepts are interconnected: in a region/season with strong coupling between soil moisture and evapotranspiration, a wet soil moisture anomaly will generate a large evapotranspiration anomaly. In the absence of precipitation, the elevated evapotranspiration will decrease the soil moisture rapidly, and consequently, the memory of the anomaly will be shorter. Conversely, a lower rate of evapotranspiration and a weaker coupling implies long memory. Regions/seasons affecting forecasts of surface climate are those that have a long enough lasting memory and a coupling high enough to generate a significant increment of evapotranspiration as a response to a wet soil moisture anomaly. Regions and seasons can thus be identified for which knowledge of soil moisture content could improve forecasts of surface climate. A related term, spinup, refers to the timespan from the starting date of a simulation that a model needs to reach a dynamical equilibrium between soil moisture and atmospheric fields, that is, when the initial bias is reduced to zero (e.g., Yang et al. 1995; Cosgrove et al. 2003).

The La Plata basin (LPB) in subtropical South America is a region where land surface processes are important for the regional hydrology and surface climate. Deep soil moisture memory has been estimated to be about 15–55 days using a suite of different land surface models driven by reanalysis (Dirmeyer et al. 2009) and up to 30 days as estimated from regional climate model (RCM) simulations of one summer season (Ruscica et al. 2014). GCM studies have shown that soil moisture–precipitation coupling is relatively strong in this region during the austral summer (Wang et al. 2007). Moreover, land–atmosphere interactions are needed in order to adequately simulate the amplitude of the precipitation anomalies as well as the correct pattern of surface temperature during El Niño episodes (Barreiro and Díaz 2011). RCM simulations for one summer season also identify LPB as a region with both strong soil moisture–evapotranspiration and soil moisture–precipitation coupling (Sörensson and Menéndez 2011). Soil moisture initial fields, particularly those that are anomalously dry, have been shown to impact the precipitation over the northern part of the basin during the early stages of the monsoon (Collini et al. 2008; Sörensson et al. 2010). These results as a whole suggest a relatively high recycling rate within the basin, in agreement with the diagnostic study of Dirmeyer and Brubaker (2007).

In this study, a single period (2 years) is used to examine the hypothesis that, to better understand the possible contributions of the soil to the seasonal predictive skill of a model, it is necessary first to investigate the processes that define the soil moisture memory and the corresponding uncertainties for different vegetation covers. The initialization of regional climate simulations with soil moisture from reanalysis data is a common practice, which inevitably generates errors since soil moisture values are not transferable from one model to another.

Several specific questions are addressed here. How does the soil moisture initialization affect predictions of surface climate over LPB? How do initial soil moisture biases evolve in time? Does interaction with the atmosphere depend on the type of land cover? How important is the choice of month of initialization for monthly to seasonal climate predictions? These questions are assessed specifically for the Weather Research and Forecasting (WRF) Model coupled with the Noah land surface model (LSM), initialized and forced at the lateral boundaries of the domain with the NCEP–NCAR reanalysis (hereafter referred to as R-1; Kalnay et al. 1996). While WRF–Noah initialized and forced at the boundaries by R-1 is a particular modeling suite, these concepts should be useful for studies with any other model configuration.

Our basic experiment uses year-long simulations to investigate the effects of soil moisture initialization over LPB for different vegetation types and seasons. Section 2 presents the methodology, experimental setup, and discussion of the control simulation. Section 3 discusses an analysis of spinup for different times of the year and different land cover types. Section 4 examines the role of soil moisture on surface temperature biases, and section 5 focuses on the surface climate processes of a simulation initialized in austral autumn. The concluding remarks are presented in section 6.

2. Methodology and modeling approach

a. The WRF and Noah

The WRF Model, version 3.2.1, is configured with a horizontal grid spacing of 36 km and 35 vertical levels over a domain covering southern South America (Fig. 1). WRF was run in climate mode using the physical configuration described and evaluated in Lee and Berbery (2012) and Müller et al. (2014). All variables needed for WRF initialization are taken from R-1, including surface variables such as soil moisture. Lateral boundary conditions are also taken from R-1 and updated every 6 h. A lateral boundary relaxation zone of 5-gridpoint width was used. Spectral nudging in the interior of the domain was not used in order to give the atmosphere more freedom to respond to the surface forcing (Pohl and Crétat 2014). Although we did not use nudging, we acknowledge its importance in studies that seek to avoid regional model

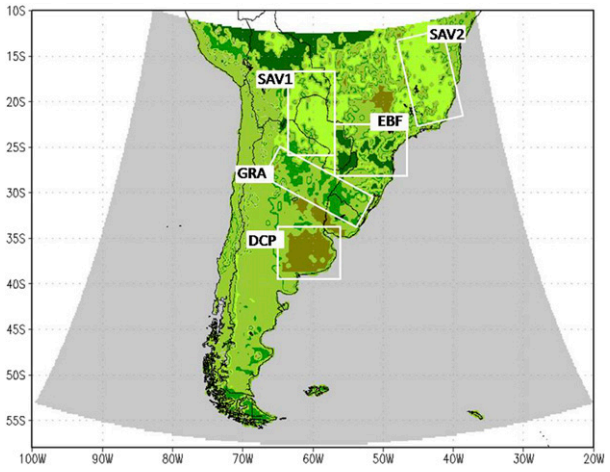

FIG. 1. Simulation domain and vegetation types considered in this study (see section 2c for acronym expansions). The vegetation-based regions are bounded by rectangles. All computations use a mask covering the respective vegetation type.

drifts from the spatial scales of the forcing global model/reanalysis, thus improving the downscaled climate and limiting the internal variability of the regional model (e.g., Miguez-Macho et al. 2005; Radu et al. 2008; Alexandru et al. 2009).

WRF is coupled to Noah, version 3.0 (Chen et al. 1996; Ek et al. 2003). Noah has four soil layers with depths of 0–10, 10–40, 40–100, and 100–200 cm. The infiltration scheme for subgrid variability follows Schaake et al. (1996). Both surface and subsurface runoff are computed, and the lower boundary condition is gravitational free drainage. Noah uses a Jarvis–Stewart canopy conductance approach and a linearized solution to the surface energy balance. Surface exchange coefficients, and thus surface fluxes, are determined via the surface layer parameterization described by Chen et al. (1997).

b. Model performance

Evaluations of the WRF precipitation have been performed over South America, in particular over LPB, in previous studies. WRF simulations realistically capture the observed pattern of the springtime precipitation fields (Lee and Berbery 2012). Magnitudes are comparable to observations in general, although some areas exhibit biases, particularly near and over mountains. Müller et al. (2014) found that the WRF Model reproduces the seasonal evolution of the observed precipitation as well as the gradients over the La Plata basin, with high values toward the northeast of the domain and decreasing toward the southwest. Lee and Berbery (2012) and Müller et al. (2014) also found good agreement in structure and northeast–southwest gradients of the observed and model temperature patterns. In La Plata basin the magnitude differences range from −1° to +1°C, although larger biases develop near mountains.

Noah has been evaluated and employed in several studies of land surface–atmosphere interactions coupled to both regional and global climate models (Koster et al. 2004; Trier et al. 2008; Dirmeyer et al. 2006; Zhang et al. 2008; Zhang et al. 2011; Chen and Zhang 2009). The coupling strength depends on the time scales and soil moisture depth employed in the corresponding definitions of land–atmosphere coupling. In the GLACE-1 studies, the coupling strength is defined by the relation between subsurface soil moisture and surface variables (Koster et al. 2006; Guo et al. 2006). Wang et al. (2007) employed the full-column soil wetness, and Wei and Dirmeyer (2012) employed the top-1-m soil wetness.

Noah has shown high evapotranspiration sensitivity to total soil moisture when coupled to the Eta Model in areas of the Mississippi basin where evapotranspiration is limited by soil moisture (Berbery et al. 2003). Noah's response to surface soil wetness/temperature is similar to other LSMs (Zhang et al. 2011); however, if subsurface soil moisture is considered, Noah exhibits weak soil moisture–temperature and evapotranspiration coupling (Koster et al. 2006; Guo et al. 2006). The weak coupling of Noah results from the use of its thicker (10 cm) first soil layer that dominates the variability of the surface fluxes (Zhang et al. 2011). Noah has also shown shorter latent heat flux memory on a global scale than two other LSMs coupled to the same GCM (Wei et al. 2010). While this was attributed to a larger fraction of vegetation interception of rainfall, the results over the La Plata basin were quite similar to the other two LSMs used. Because of the variety of definitions, our reference to coupling will not be tied to a specific one, but rather to the general concept that links land surface and atmosphere.

c. Vegetation types

The default Noah land cover categories are obtained from the U.S. Geological Survey (USGS) global 1-km land cover map (Anderson et al. 1976). The USGS database consists of 24 land surface categories, and each one is associated with a set of physical parameters defined through a lookup table in the Noah model. Four vegetation types of Noah–USGS that cover most of LPB will be discussed here: savanna (SAV); evergreen broadleaf forest (EBF); grassland (GRA); and dryland, cropland, and pasture (DCP). The savanna vegetation type was divided in two subregions (SAV1 and SAV2) because they are geographically apart. Figure 1 presents the regions corresponding to each vegetation type bounded by rectangles. All computations were done using masks over the specific land cover.

TABLE 1. Mean soil and vegetation parameters for the vegetation-based regions.

	SAV1	SAV2	EBF	GRA	DCP
Field capacity (volumetric fraction)	0.35	0.37	0.38	0.38	0.38
Wilting point (volumetric fraction)	0.08	0.1	0.11	0.1	0.1
No. of soil moisture layers with roots	3	3	4	3	3
Stomatal resistance ($s\,m^{-1}$)	70	70	150	40	40
Roughness length [yearly mean (m)]	0.15	0.15	0,5	0,11	0.1

Biophysical parameters corresponding to the five regions are summarized in Table 1. In the Noah model, the wilting point and the field capacity (minimum and maximum water content of the soil) are the soil parameters that influence the water-holding capacity, that is, the maximum water content in the soil column. Table 1 indicates that the range wilting point–field capacity is relatively similar for all regions, with SAV1 having the lowest wilting point value but also the lowest field capacity. Note that for the SAV1 and SAV2 regions, wilting point and field capacity have slightly different values because they have different soil properties. Root depth, measured in soil layers, depends on the vegetation type. EBF has roots in all four layers in contrast to the other vegetation types that have roots only in the upper three layers. This means that EBF is the only case in which the deepest layer is connected to the atmosphere through root extraction of water and transpiration. In addition, EBF has the highest roughness length, which contributes to higher evapotranspiration capacity. However, its stomatal resistance is also higher, acting to constrain the evapotranspiration.

The seasonal cycles of leaf area index (LAI) and albedo are presented in Fig. 2. Albedo is the fraction of incoming radiation that is reflected from the surface; thus, it determines the amount of energy that is available for the total heat flux (sensible and latent). Large annual amplitudes of albedo with minimum values during austral winter are found over SAV, GRA, and DCP (Fig. 2a). EBF, in contrast, has constant and low values throughout the year. LAI, which positively influences the evapotranspiration capacity, achieves the largest values during austral spring for DCP and during austral summer for SAV and EBF (Fig. 2b). LAI's lowest yearly mean and annual amplitude are found over the GRA vegetation type.

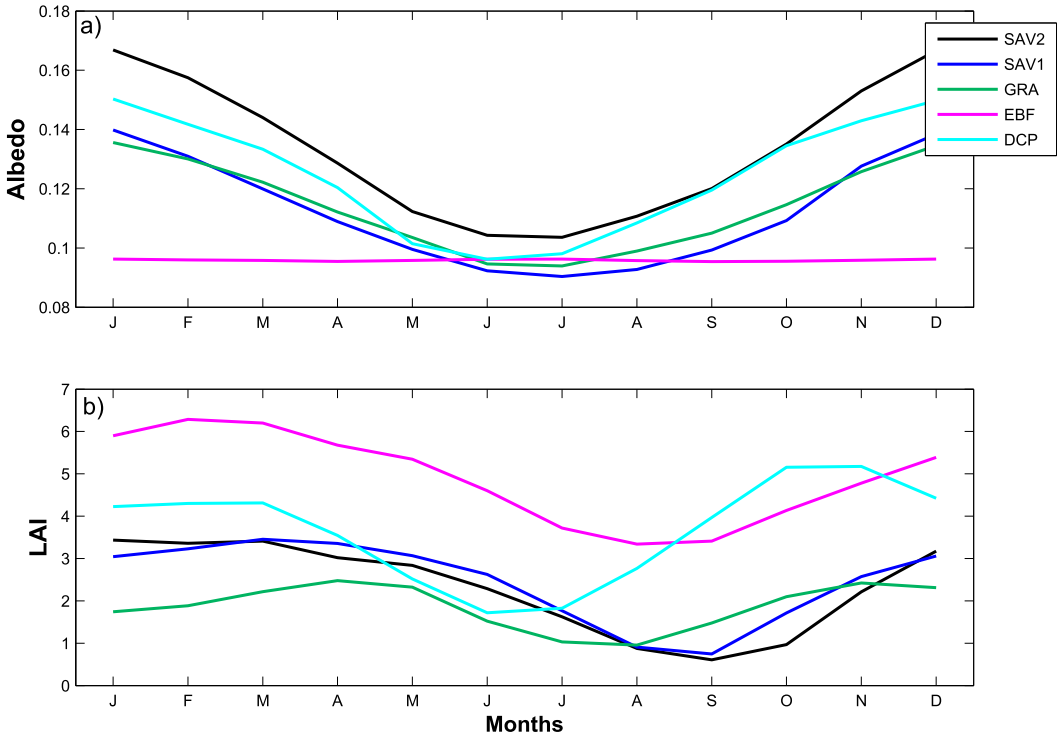

FIG. 2. (a) Albedo and (b) LAI seasonal cycles.

d. Experimental setup

Our study is designed to offer a conceptual discussion of the physical processes involved in the soil moisture–atmosphere interactions. First, a 3-yr simulation is carried out using R-1 atmospheric and soil variables for WRF initialization. Lateral boundary conditions updated every 6 h are also taken from R-1. The simulation starts on 1 January 2000 and ends on 31 December 2002. Following Cosgrove et al. (2003), the first year is considered a spinup period for the soil moisture, which reaches equilibrium with the atmosphere by 1 January 2001. From now on we will refer to the simulation's 2-yr period from 1 January 2001 to 31 December 2002 as the control (CTL) experiment. This period had neutral-to-moderate El Niño–Southern Oscillation conditions, and therefore, possible effects from remote forcings should be less relevant.

To address the questions posed in the introduction and understand the evolution of soil moisture and surface variables as a function of the vegetation type and time of the year, and recognizing that R-1 has a strong soil moisture annual cycle, a sensitivity test of the WRF–Noah suite is carried out. Twelve 1-yr-long simulations (EXP simulations) starting on the first day of each month during 2001 are performed. As with CTL, all EXP simulations use R-1 for initialization, including soil moisture, and forcing at the lateral boundaries. [The spinup time of the initial atmospheric states is not considered as their time scales are of about 1–10 days (see, e.g., Seth and Giorgi 1998; de Elía et al. 2002; Denis et al. 2002; Laprise 2008).] The 12 EXP simulations cover the same period of the CTL simulation, and this 2-yr period ensures that there will be multiple individual episodes to cover a variety of processes during the spinup time of the EXP soil moisture. Despite having multiple single episodes, this approach is not intended to assess the statistical significance of the results. The differences in soil moisture and other surface variables between CTL and the EXP simulations are hereafter called dry/wet biases, or differences, of the EXP simulation.

e. WRF Model initialization with R-1 soil moisture

The initial soil moisture conditions of the EXP simulations are interpolated from R-1's two layers to Noah's four layers, which introduces different sources of error. First, a model's soil moisture values are thought of as model-dependent indices and not as actual soil water content that can be compared with in situ measurements or even against other model estimates (see, e.g., Koster et al. 2009). Second, even if the soil moisture indices were exchangeable, the soil moisture on a specific date would still differ between the two simulations because the atmospheric component of the two different models (R-1 and WRF in this case) would produce different amounts and distribution of precipitation preceding the forecast initial date. After a certain spinup time, the land surface and atmospheric states in the WRF simulations will reach a balance that will be different from the one in R-1.

Figure 3 contrasts the evolution of soil moisture in the EXP simulations against those from the CTL experiment during year 2001 (which is in equilibrium after the 1-yr spinup). The EXP initial values are noted by colored dots in the figure and are only the R-1 soil moisture interpolated to the four Noah layers at the beginning of each month. Figure 3 (left) presents the soil moisture in the first layer (SM1), while Fig. 3 (right) depicts the soil moisture in the fourth layer (SM4). The second and third layers (SM2 and SM3) are not shown, as in all cases their evolution is similar to that of SM1, although with a slower response to rainfall, lagging by about 2 days for SM2 and by 1–2 weeks for SM3. The land surface model used in R-1 employs nudging to the surface climate with the purpose of avoiding long-term drifts, which leads to noticeable amplitudes of the annual water content, in particular in the deep layer (Roads and Betts 2000; Betts et al. 1998; Li et al. 2005). The EXP values of SM4 are similar to those in SM1 because of R-1's nudging to the surface climate. In contrast, SM1 and SM4 of CTL show much less similarity because WRF–Noah does not use nudging and the soil moisture therefore evolves without restrictions. In the case of LPB this effect is clearly noticed in the SAV1 region (Figs. 3a,b) but is also present in the other vegetation types.

3. Memory processes

The convergence of soil moisture in each EXP simulation toward the CTL depends on the time of the year and type of land cover. In addition to the temporal evolution of soil moisture for the continuous CTL simulation, Fig. 3 presents the twelve 1-yr EXP simulations starting at the beginning of each month of 2001. (All EXP simulations, except the one started in January 2001, extend into 2002. The equivalent of Fig. 3 for the year 2002 is not presented as it does not add substantial information.)

a. Savanna

The SAV regions have a marked annual cycle of precipitation related to the South American monsoon, with a dry season in austral autumn and winter, and heavy rainfall during spring and summer (Zhou and Lau 1998; Berbery and Barros 2002; Nogués-Paegle et al. 2002; Marengo et al. 2012). The Savanna biophysical

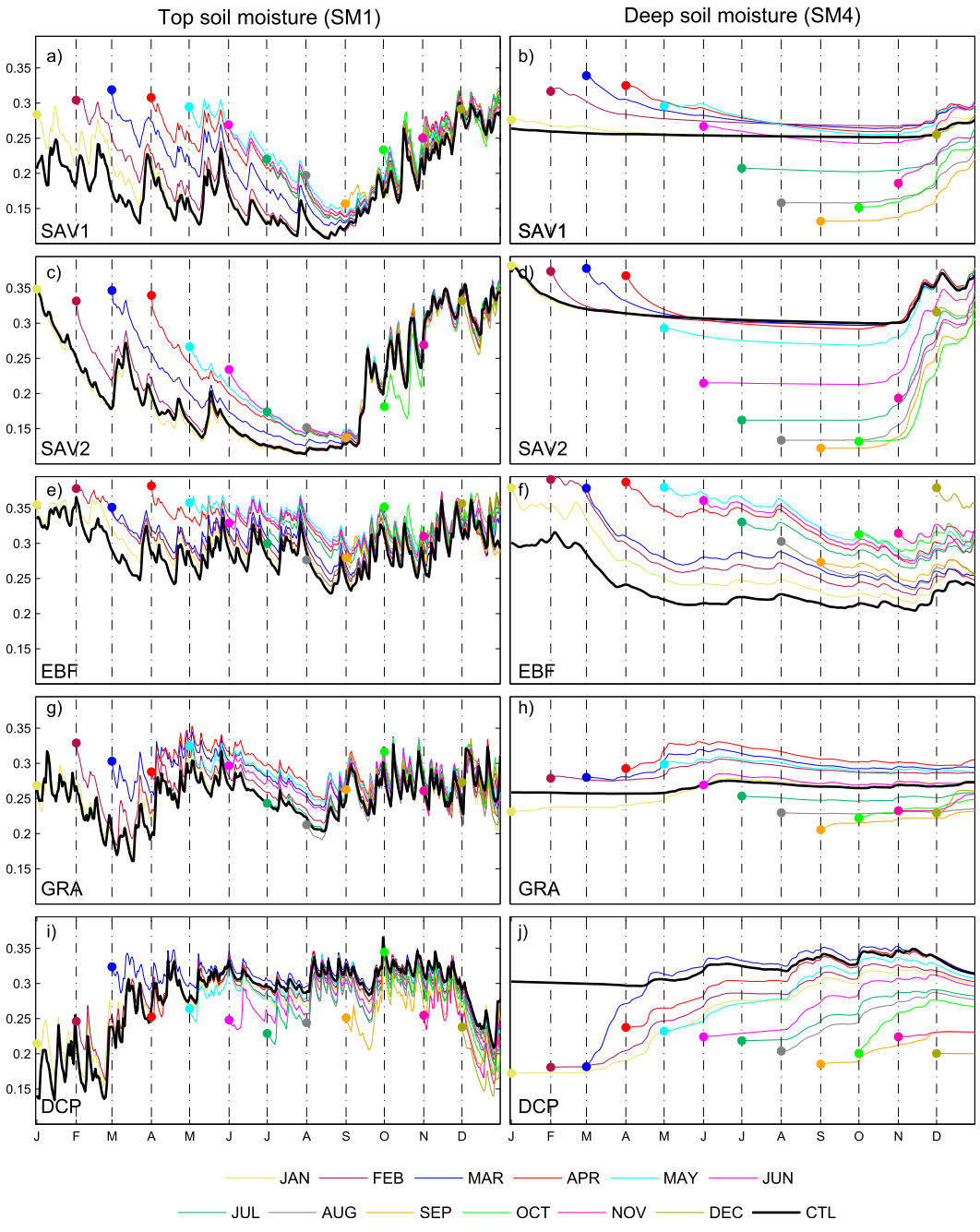

FIG. 3. Top and deep soil moisture 2001 evolution for the CTL simulation and the 12 EXP simulations.

parameters have intermediate values compared to the other LPB vegetation types (see Table 1, Fig. 2), suggesting that the evapotranspiration capacity and total heat fluxes are lower than in the EBF region during the whole year. During austral spring, the SAV region has a considerably lower LAI, leading to lower evapotranspiration capacity.

Figures 3a and 3c show that the SM1 of both the CTL and EXP simulations of the two SAV regions have a marked annual cycle where the EXP simulations have a large initial wet bias from austral summer until early spring (as shown by the color dots indicating the EXP initial values). The wet initial biases in the three upper layers during this period are removed through higher transpiration from root extraction of moisture (SM2 and SM3 are not shown). When rain starts in austral spring (September–October) the soil is dry and able to absorb water; hence, the upper three layers of both simulations

are gradually filled with water. As a result, the memory of the upper layer is lost after about 1 month, and the same behavior is found for the second layer but not for the third one, where memory persists for several months, contributing to the evapotranspiration (not shown).

The water content of the fourth layer in the CTL simulation (black solid line in Figs. 3b,d) has reached an equilibrium value and is almost constant during the year. Since the R-1 deep soil moisture is nudged to the top soil moisture, initial values of SM4 in the EXP simulations (Figs. 3b,d) exhibit a marked annual cycle that is similar to that in SM1. Because of the lack of roots in SM4, water in this layer is not used for evapotranspiration, even when water levels are high. Instead, it is discharged as underground runoff until water levels adjust to the equilibrium value $0.26\,m^3\,m^{-3}$ (not shown). Figures 3b and 3d also indicate that when the fourth layer is initialized very dry during winter, the dry biases will remain unchanged until the end of October, when water reaches that layer by percolation. Therefore, the fourth-layer dry/wet biases do not affect the simulated surface climate, that is, there is no coupling between the fourth layer and the atmosphere.

b. *Evergreen broadleaf forest*

Rainfall in the EBF region is frequent throughout year, but with more intensity during austral summer (e.g., Berbery and Barros 2002; Grimm 2003). Figure 3e shows that the initial biases of the top layer are wet throughout the year. Both the EXP and the CTL simulations have a weak annual cycle and the soil water remains quite close to saturation. Since this is the region with the densest forest, the albedo is lowest and more solar energy is absorbed that will be available for surface fluxes. As stated in section 2c, EBF evapotranspiration is larger in part because water can be extracted from all four layers and because of the high LAI and roughness length. However, the response of evapotranspiration to wet soil moisture biases is low because of the abundance of soil water and thus is only limited by atmospheric energy. Variability in the fourth layer's soil moisture is evidence of the extraction of water for evapotranspiration as a result of the deeper roots (Fig. 3f).

The fourth layer's water amounts in the CTL simulation are lower than in the other vegetation types because of the deep-layer root extraction of water for evapotranspiration. All EXP simulations show that the soil moisture in all layers is initialized too wet throughout the year, and these biases adjust slowly to equilibrium values. This is a situation where the soil moisture memory is high since wet anomalies do not noticeably affect the atmosphere, and the coupling with the atmosphere is therefore low.

c. *Grasslands*

The GRA vegetation parameters (Table 1, Fig. 2) suggest a low evapotranspiration capacity since the roughness length and the LAI are the lowest of all vegetation types, despite a partial compensation by the lower stomatal resistance. Figures 3g and 3h indicate that the EXP initial biases of the upper layer (and of SM2 and SM3, not shown) are wet for the first half of the year and almost neutral for the second half. During the cold season, the lower temperatures and potentially the lower LAI (recall Fig. 2) contribute to lower soil moisture depletion than, for example, the SAV regions. During the austral summer, rainfall is more intense; nevertheless, the soil dries out because of high temperatures. Consequently, the top-layer soil moisture has two local minima during the year. The lack of deep roots prevents the extraction of water for evapotranspiration, and therefore, this layer's memory is very long. The equilibrium soil moisture in the fourth layer is almost constant, as it had been noticed in the SAV1 region. Yet, the annual amplitude of EXP initial values and the initial biases are lower than in SAV1.

d. *Dryland, cropland, and pasture*

The DCP region has a weak annual cycle of precipitation, with slightly higher precipitation in austral summer (Berbery and Barros 2002). It is shown in Fig. 2 that during spring and summer DCP has high LAI values, which, together with the high summer temperature, favor evapotranspiration, resulting in the depletion of soil moisture and drying out of the upper layer (Fig. 3i). Unlike for the other vegetation types, the EXP simulations underestimate the initial soil moisture for almost all months, that is, the initial soil state is drier in EXP than in the CTL simulation. In these cases, and since rain falls throughout the year, soil moisture memory of the upper layer is lost after 1–2 months (Fig. 3i). In the case of the fourth layer (Fig. 3j), the initial values are 30%–50% lower than the equilibrium CTL values during the entire year. The percolation of rainfall to the fourth layer adjusts the EXP simulations to the CTL curve, but this process takes several months. Once rainfall reaches to the fourth layer, it ceases to be available for evapotranspiration because of the lack of roots.

e. *Water in the soil column*

To provide a clearer picture of how water is evapotranspirated and recharged in the soil column, Fig. 4 presents the CTL simulation precipitation and the soil moisture evolution of all four layers for SAV1 and EBF during the year 2001. Values are slightly smoothed using 5-day averages. SAV1 was selected as an example of

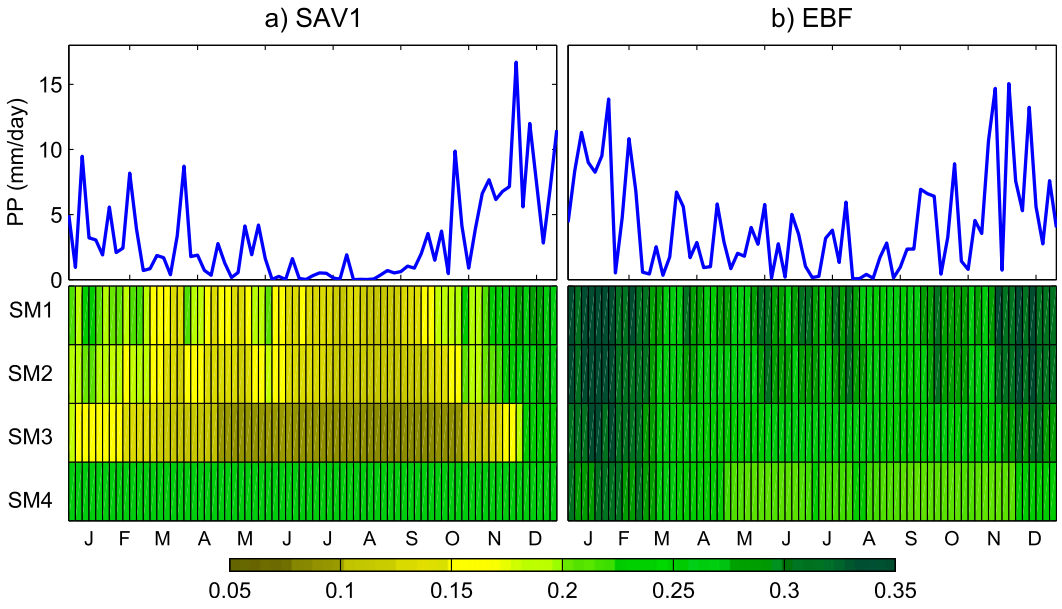

FIG. 4. Time evolution of precipitation and soil moisture for the CTL simulation during 2001: (a) SAV1 and (b) EBF. Pentads (5-day averages) are used for a slight smoothing.

a region with roots that only reach the third layer, while EBF is chosen because its roots reach the fourth layer. The three upper layers of SAV1, particularly the third one, dry out during the dry period (Fig. 4a). The fourth layer, without a mechanism to extract water to the atmosphere, remains saturated. On the contrary, the EBF fourth layer interacts with the atmosphere through evapotranspiration, thus showing a decrease in time of moisture content (Fig. 4b). Figure 4 also gives a sense of the time scale of the recharge of each layer after precipitation events, in particular during the rainy period (September–December). Infiltration of water to deeper layers depends directly on the precipitation amount and inversely on the evapotranspiration from SM1, which in turn depends not only on soil water content temperature and atmospheric moisture content (see next section). The recharge of the upper layer is not a linear response to the rainfall amount, since heavy rainfall generates a larger surface runoff than lighter rain during a longer period.

4. Role of soil moisture on surface temperature biases

Surface climate is sensitive to soil moisture in climate regimes that are neither very dry nor very wet (transitional climate regimes; e.g., Koster et al. 2004). In a transitional climate regime, soil moisture is the main controlling factor of the partitioning of total surface energy in sensible and latent heat fluxes, and consequently also on the near-surface temperature and on the evapotranspiration. On the contrary, in wet climate regimes, the partitioning of fluxes is governed by atmospheric moisture demand that is mostly controlled by surface radiation. In either case, surface temperature and evapotranspiration also depend on how much energy is available for total surface fluxes, which is controlled by radiation and clouds. In this sense, precipitation is important for surface temperatures because of its direct and strong influence on soil moisture and because of its correlation with cloud cover. In our experiments, the soil moisture biases are in many cases large and persistent and can become important for surface temperature and climate. Since total fluxes reach their maximum values during daytime, soil moisture should affect the maximum 2-m temperature $T_{2\mathrm{mX}}$ to a larger degree than the minimum 2-m temperature $T_{2\mathrm{mN}}$. This section will focus specifically on the relation between soil moisture biases and $T_{2\mathrm{mX}}$ biases.

Figure 5 presents the relationship between monthly mean area-averaged top-layer soil moisture biases and the $T_{2\mathrm{mX}}$ biases. Each point in the figure corresponds to the monthly mean of each simulation, giving a total of 36 points per season (12 simulations $\times$ 3 months per season). The corresponding correlations between the two variables are shown in Table 2. The two savanna regions and the EBF region have annual correlations of soil moisture with $T_{2\mathrm{mX}}$ of -0.97, -0.96, and -0.93, respectively. The EBF region (Fig. 5c) has a smaller SM1 intra-annual spread (as also seen in Fig. 3e), although the biases are only somewhat smaller than in the SAV regions. The GRA and DCP regions (Figs. 5d,e) show a somewhat weaker relationship between SM1 and $T_{2\mathrm{mX}}$

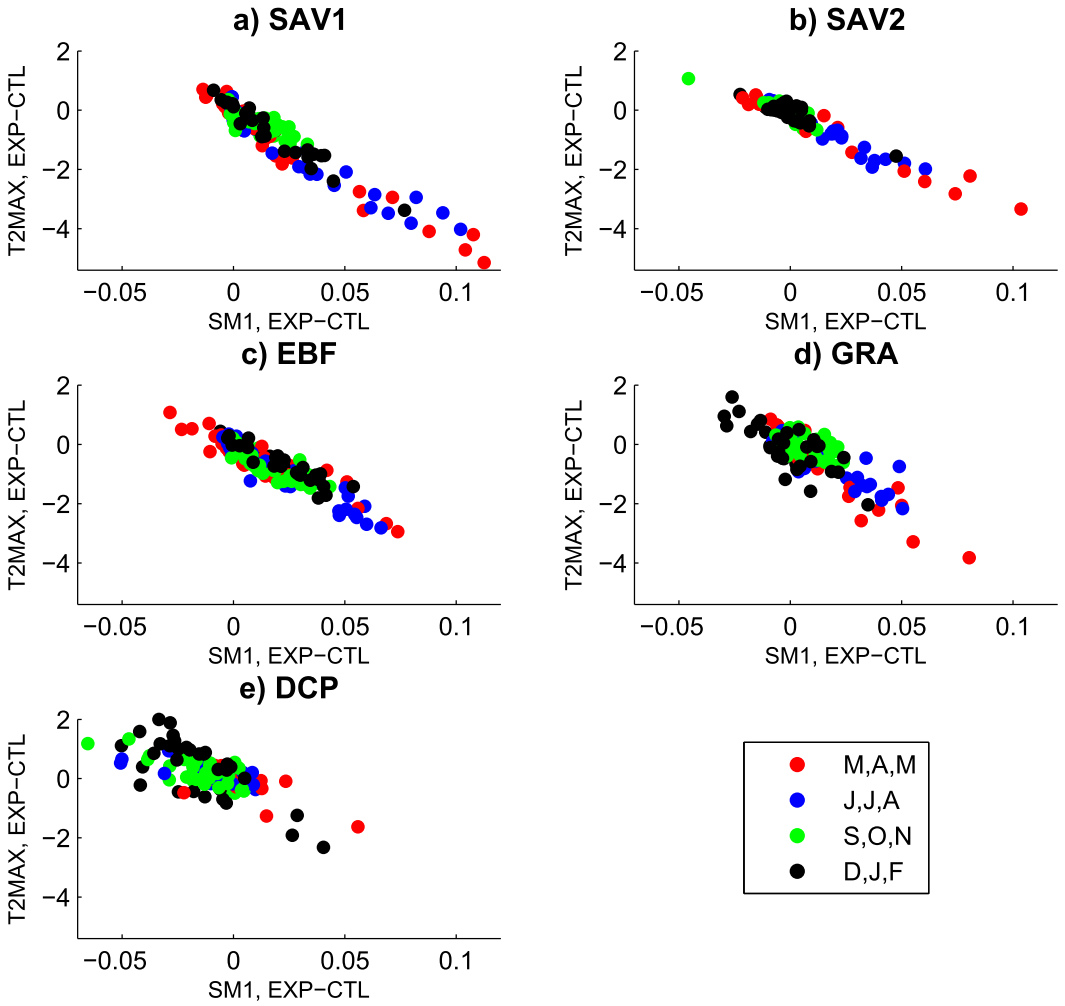

FIG. 5. Monthly mean top soil moisture (SM1) bias vs monthly mean T_{2mX} bias. Colors indicate season: austral autumn is red, winter is blue, spring is green, and summer is black.

biases, with the lowest correlation (−0.46) occurring in austral spring in GRA. These weaker correlations indicate that the T_{2mX} biases depend on other processes, for example, the CTL and EXP differences in cloudiness and net radiation (see Betts and Viterbo 2005; Seneviratne et al. 2010). Since CTL and EXP only differ in their initial date and initial soil moisture, these differences are assumed to be due to internal variability of cloudiness or soil moisture feedbacks.

5. Surface climate processes

The processes at the surface that are most related to soil moisture variability are examined next. The simulation initialized on 1 April 2001 and ending on 31 March 2002 (EXP4) was chosen to focus on a time when the soil moisture initial biases are large. The results are presented for a region with a well-defined dry season (SAV1) and another region with a nondescript annual cycle (EBF). Five-day means are used to remove high-frequency variability.

a. *SAV1 region*

The precipitation of the CTL simulation (Fig. 6a) indicates that rainfall is initially weak and interspersed by dry periods lasting from days to weeks until October,

TABLE 2. Correlations of monthly top soil moisture (SM1) bias and monthly mean T_{2mX} bias on yearly and seasonal [December–February (DJF), March–May (MAM), June–August (JJA), and September–November (SON)] time scales.

	SAV1	SAV2	EBF	GRA	DCP
Yearly	−0.97	−0.96	−0.93	−0.84	−0.73
DJF	−0.97	−0.87	−0.92	−0.76	−0.76
MAM	−0.98	−0.98	−0.94	−0.94	−0.72
JJA	−0.97	−0.97	−0.96	−0.89	−0.66
SON	−0.79	−0.87	−0.84	−0.46	−0.74

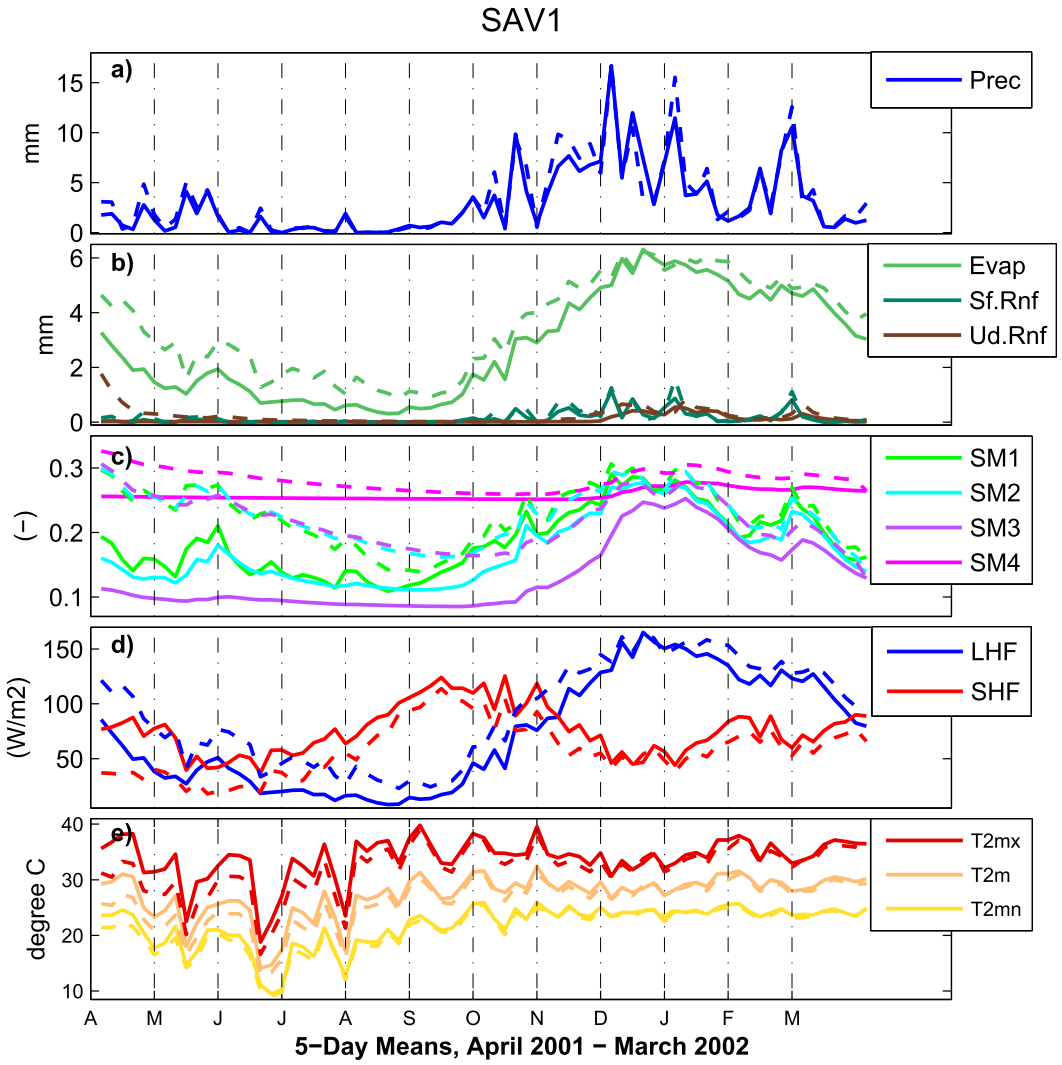

FIG. 6. The 5-day-mean evolution of the SAV1 variables relevant for the water balance: (a) precipitation, (b) evaporation and runoff, (c) soil moisture, (d) heat fluxes, and (e) 2-m temperature for the CTL simulation and the EXP4 simulation initialized in April. Solid lines show CTL values and dashed lines represent the EXP4 results.

when the rainy season starts. Until December the precipitation in the EXP4 simulation exhibits a noticeable similarity with that of the CTL simulation (Fig. 6a), indicating that internal variability of precipitation is low and that the atmospheric boundary conditions exert a strong influence on rainfall. This is in contrast with the evolution of soil moisture (Fig. 6c), particularly in the first few months, when the EXP4 initial soil moisture in the three upper layers is about 2–3 times higher than the CTL values. The similarity in precipitation evolution and the dissimilarity in soil moisture evolution suggest weak soil moisture feedbacks. Any extra water in the upper three layers is partitioned between evapotranspiration and drainage, while SM1 has the additional contribution to surface runoff (Fig. 6b). Figure 6c shows that both SM3 and SM4 of the CTL simulation are constant until late austral spring. Water does not reach the third layer, since the sparse precipitation is employed by the first two layers for evapotranspiration. Without roots, the fourth layer does not contribute to the evapotranspiration at any time. Instead, water reaching the fourth layer is lost as underground runoff when the water level is higher than the equilibrium level ($\sim 0.26\,m^3\,m^{-3}$).

The evolution of CTL evapotranspiration and latent heat flux (Figs. 6b,d) closely follows that of the top soil moisture (Figs. 6c). Because of the higher availability of soil water, the EXP4 evapotranspiration and the latent heat flux exhibit large positive differences with respect to the CTL experiment during the first months. The sensible heat flux behaves like a mirror image of the latent heat flux, leading to lower temperatures in the EXP4 simulation (Fig. 6e).

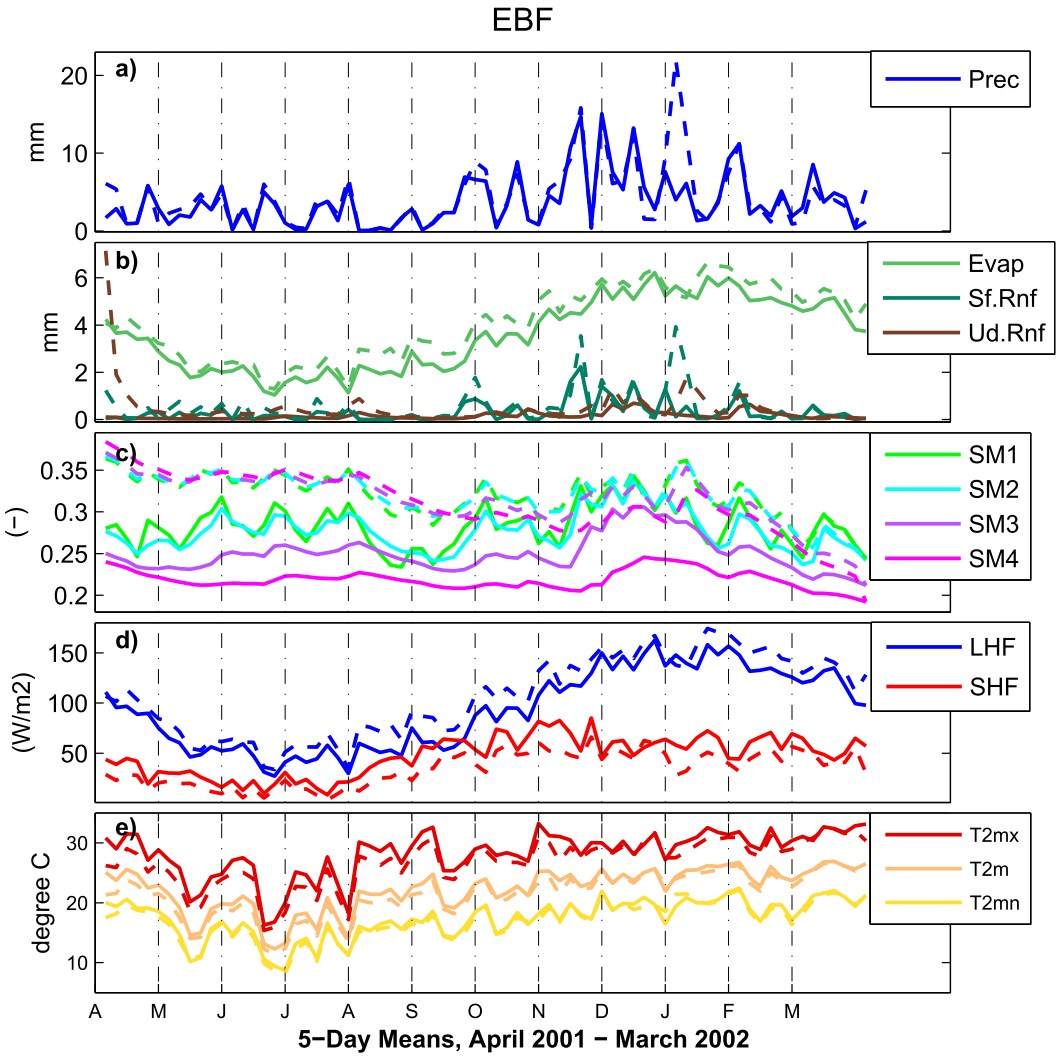

FIG. 7. As in Fig. 6, but for EBF.

In summary, the close agreement between the CTL and EXP4 precipitation suggests a strong influence of the atmospheric boundary conditions. Small differences in amplitude can be attributed to internal variability or other external factors. During the dry period, the EXP4 soil moisture adjusts to the CTL values through evapotranspiration from the upper three layers, which are coupled to the atmosphere. The dry period is not sufficiently long for the EXP4 soil moisture to reach equilibrium values. However, when the rainy period starts in October, the two simulations converge, since excess water of the EXP4 soil is assigned to either surface or underground runoff while the drier CTL soil is filled with water.

b. *EBF region*

This region has a subtropical forest behavior with high soil water levels and a large evaporative fraction as discussed earlier. Figure 7a shows that rainfall during the cold season (May–September) is frequent but not as large as during the warm season (October–February). The initial soil moisture of EXP4 is about 50% higher than in CTL (Fig. 7c). However, Figs. 7b and 7d show that the evapotranspiration (latent heat flux) of the two runs differ less than in the SAV1 region during the first months, indicating that the vapor pressure deficit is lower in EBF than in SAV1. This implies that the partitioning of the surface fluxes is controlled by the atmosphere to a higher degree and by the soil moisture to a lesser extent. As a consequence, the differences in temperatures are much smaller than in the SAV1 region (Fig. 7e, note differences in scale on the *y* axis) Starting in August, the warmer atmosphere favors higher latent heat flux in the wetter EXP4. Then, the soil moisture of EXP4 starts to adjust toward the CTL equilibrium soil moisture. When

rainfall becomes more intense in October, the CTL soil moisture of the third and fourth layers increases, gradually eliminating the initial difference between the two simulations.

6. Concluding remarks

The impact of soil moisture initialization with different land cover types and for different seasons in the La Plata basin was assessed with the WRF–Noah–R-1 modeling suite. Results suggest that the seasonal predictive skill over LPB is higher when the modeling suite is initialized during the wet season (September–January) when the initial differences between CTL and EXP, which is initialized with R-1, are small. On the contrary, during the dry season (February–August), the soil is much wetter in the EXP simulations than the WRF–Noah equilibrium soil moisture, and the adjustment to equilibrium values is slow, indicating a long memory.

Uncertainty in the simulated maximum surface temperature, which can amount to several degrees Celsius, originates from initial soil moisture biases regardless of the vegetation type.

In the case of EBF, roots reach the fourth soil layer, and the whole soil moisture column influences the partitioning of the surface fluxes that affect the surface temperature. Roots in the other vegetation types do not reach the fourth layer; therefore, the partitioning of surface fluxes is only influenced by soil moisture in the upper three layers.

It is found that the impact of a wet initialization depends on the region, season, and vegetation type. When the model is initialized with too-high soil moisture values during a relatively wet season, a vegetation type with limitations on its evapotranspiration (in LPB's case, the EBF region) will have a low rate of adjustment to equilibrium values, and consequently, the wet initialization will not affect the surface climate much. A situation where the model's soil moisture is initialized too wet during a dry season (e.g., the SAV1 region) will show a faster adjustment, which implies higher interaction with the atmosphere. Previous studies have examined the influence on the surface climate and/or atmospheric processes of dry versus wet initial soil moisture conditions defined uniformly for a large simulation domain, for example, as a percentage of the initial value given by the driving model (Collini et al. 2008; Sörensson et al. 2010), a percentage of field capacity (Rodell et al. 2005), or a percentage of the equilibrium soil moisture values (Barthlott and Kalthoff 2011). Our study shows that wet and dry initializations can be better defined depending on the characteristics of a particular region and season, rather than on a definition that considers a fixed fraction of the initial or equilibrium soil moisture.

The effects of the initial differences in soil moisture can also be delayed when an initial bias persists during a season with limited interaction with the atmosphere. As the soil starts to interact with the atmosphere, the effect of this bias is detected in surface variables such as evapotranspiration and temperature. This was seen in the EBF region, where the large wet biases only contribute to large evapotranspiration biases when the total energy available for fluxes is sufficient. It was shown that, consistent with the results of Koster and Suarez (2001), seasons with heavy rainfall that are forced by large-scale circulation can remove the soil moisture memory, and thus, the initial soil moisture would not contribute to the predictability of surface climate of subsequent months. The soil moisture memory and the interaction with the atmosphere depend thus on the difference of the initial values from equilibrium values and on the moisture–atmospheric regime at the time of initialization.

The present study centered on the period 2001–02, which includes multiple precipitation episodes, each with a given impact on soil moisture and land–atmosphere processes. Admittedly, a longer period and an ensemble approach are desirable to define metrics and assess the statistical significance of the results (i.e., their robustness). Since this study employs only one modeling suite, the results may be different for other combinations of atmospheric models, land surface models, and reanalyses. However, the intent here was to offer a conceptual analysis of the processes involved during the adjustment stages of long-term simulations.

Acknowledgments. We thank the anonymous reviewers for their thoughtful comments. This research was supported by NASA Grant NNX08AE50G and by the Inter-American Institute for Global Change Research (IAI) through the Cooperative Research Networks CRN-2094 and CRN-3095.

REFERENCES

Alexandru, A., R. de Elía, R. Laprise, L. Separovic, and S. Biner, 2009: Sensitivity study of regional climate model simulations to large-scale nudging parameters. *Mon. Wea. Rev.,* **137,** 1666–1686, doi:10.1175/2008MWR2620.1.

Anderson, J. R., E. E. Hardy, J. T. Roach, and R. E. Witmer, 1976: A land use and land cover classification system for use with remote sensor data. USGS Professional Paper 964, 28 pp. [Available online at http://pubs.usgs.gov/pp/0964/report.pdf.]

Barreiro, M., and N. Díaz, 2011: Land–atmosphere coupling in El Niño influence over South America. *Atmos. Sci. Lett.,* **12,** 351–355, doi:10.1002/asl.348.

Barthlott, C., and N. Kalthoff, 2011: A numerical sensitivity study on the impact of soil moisture on convection-related parameters and convective precipitation over complex terrain. *J. Atmos. Sci.,* **68,** 2971–2987, doi:10.1175/JAS-D-11-027.1.

Berbery, E. H., and V. R. Barros, 2002: The hydrologic cycle of the La Plata basin in South America. *J. Hydrometeor.,* **3,** 630–645, doi:10.1175/1525-7541(2002)003<0630:THCOTL>2.0.CO;2.

——, Y. Luo, K. E. Mitchell, and A. K. Betts, 2003: Eta Model estimated land surface processes and hydrologic cycle of the Mississippi basin. *J. Geophys. Res.,* **108,** 8852, doi:10.1029/2002JD003192.

Betts, A. K., and P. Viterbo, 2005: Land-surface, boundary layer, and cloud-field coupling over the southwestern Amazon in ERA-40. *J. Geophys. Res.,* **110,** D14108, doi:10.1029/2004JD005702.

——, ——, A. Beljaars, H.-L. Pan, S.-Y. Hong, M. Goulden, and S. Wofsy, 1998: Evaluation of land-surface interaction in ECMWF and NCEP/NCAR reanalysis models over grassland (FIFE) and boreal forest (BOREAS). *J. Geophys. Res.,* **103,** 23 079–23 085, doi:10.1029/98JD02023.

Chen, F., and Y. Zhang, 2009: On the coupling strength between the land surface and the atmosphere: From viewpoint of surface exchange coefficients. *Geophys. Res. Lett.,* **36,** L10404, doi:10.1029/2009GL037980.

——, and Coauthors, 1996: Modeling of land surface evaporation by four schemes and comparison with FIFE observations. *J. Geophys. Res.,* **101,** 7251–7268, doi:10.1029/95JD02165.

——, Z. Janjić, and K. Mitchell, 1997: Impact of atmospheric-surface layer parameterizations in the new land surface scheme of the NCEP mesoscale Eta numerical model. *Bound.-Layer Meteor.,* **85,** 391–421, doi:10.1023/A:1000531001463.

Collini, E. A., E. H. Berbery, V. R. Barros, and M. E. Pyle, 2008: How does soil moisture influence the early stages of the South American monsoon? *J. Climate,* **21,** 195–213, doi:10.1175/2007JCLI1846.1.

Cosgrove, B. A., and Coauthors, 2003: Land surface model spin-up behavior in the North American Land Data Assimilation System (NLDAS). *J. Geophys. Res*., **108,** 8845, doi:10.1029/2002JD003316.

de Elía, R., R. Laprise, and B. Denis, 2002: Forecasting skill limits of nested, limited-area models: A perfect-model approach. *Mon. Wea. Rev.,* **130,** 2006–2023, doi:10.1175/1520-0493(2002)130<2006:FSLONL>2.0.CO;2.

Denis, B., R. Laprise, D. Caya, and J. Côté, 2002: Downscaling ability of one-way nested regional climate models: The Big-Brother Experiment. *Climate Dyn.,* **18,** 627–646, doi:10.1007/s00382-001-0201-0.

Dirmeyer, P. A., 2000: Using a global soil wetness dataset to improve seasonal climate simulation. *J. Climate,* **13,** 2900–2922, doi:10.1175/1520-0442(2000)013<2900:UAGSWD>2.0.CO;2.

——, and K. L. Brubaker, 2007: Characterization of the global hydrologic cycle from a back-trajectory analysis of atmospheric water vapor. *J. Hydrometeor.,* **8,** 20–37, doi:10.1175/JHM557.1.

——, R. D. Koster, and Z. Guo, 2006: Do global models properly represent the feedback between land and atmosphere? *J. Hydrometeor.,* **7,** 1177–1198, doi:10.1175/JHM532.1.

——, C. A. Schlosser, and K. L. Brubaker, 2009: Precipitation, recycling, and land memory: An integrated analysis. *J. Hydrometeor.,* **10,** 278–288, doi:10.1175/2008JHM1016.1.

Ek, M. B., K. E. Mitchell, Y. Lin, E. Rogers, P. Grunmann, V. Koren, G. Gayno, and J. D. Tarpley, 2003: Implementation of Noah land surface model advances in the National Centers for Environmental Prediction operational mesoscale Eta Model. *J. Geophys. Res.,* **108,** 8851, doi:10.1029/2002JD003296.

Grimm, A. M., 2003: The El Niño impact on the summer monsoon in Brazil: Regional processes versus remote influences. *J. Climate,* **16,** 263–280, doi:10.1175/1520-0442(2003)016<0263:TENIOT>2.0.CO;2.

Guo, Z., and Coauthors, 2006: GLACE: The Global Land–Atmosphere Coupling Experiment. Part II: Analysis. *J. Hydrometeor.,* **7,** 611–625, doi:10.1175/JHM511.1.

Kalnay, E., and Coauthors, 1996: The NCEP/NCAR 40-Year Reanalysis Project. *Bull. Amer. Meteor. Soc.,* **77,** 437–471, doi:10.1175/1520-0477(1996)077<0437:TNYRP>2.0.CO;2.

Koster, R. D., and M. J. Suarez, 2001: Soil moisture memory in climate models. *J. Hydrometeor.,* **2,** 558–570, doi:10.1175/1525-7541(2001)002<0558:SMMICM>2.0.CO;2.

——, and Coauthors, 2004: Regions of strong coupling between soil moisture and precipitation. *Science,* **305,** 1138–1140, doi:10.1126/science.1100217.

——, and Coauthors, 2006: GLACE: The Global Land–Atmosphere Coupling Experiment. Part I: Overview. *J. Hydrometeor.,* **7,** 590–610, doi:10.1175/JHM510.1.

——, Z. Guo, R. Yang, P. A. Dirmeyer, K. Mitchell, and M. J. Puma, 2009: On the nature of soil moisture in land surface models. *J. Climate,* **22,** 4322–4335, doi:10.1175/2009JCLI2832.1.

——, and Coauthors, 2010: Contribution of land surface initialization to subseasonal forecast skill: First results from a multi-model experiment. *Geophys. Res. Lett.,* **37,** L02402, doi:10.1029/2009GL041677.

Laprise, R., 2008: Regional climate modelling. *J. Comput. Phys.,* **227,** 3641–3666, doi:10.1016/j.jcp.2006.10.024.

Lee, S.-J., and E. H. Berbery, 2012: Land cover change effects on the climate of the La Plata Basin. *J. Hydrometeor.,* **13,** 84–102, doi:10.1175/JHM-D-11-021.1.

Li, H., A. Robock, S. Liu, X. Mo, and P. Viterbo, 2005: Evaluation of reanalysis soil moisture simulations using updated Chinese soil moisture observations. *J. Hydrometeor.,* **6,** 180–193, doi:10.1175/JHM416.1.

Marengo, J., and Coauthors, 2012: Recent developments on the South American monsoon system. *Int. J. Climatol.,* **32,** 1–21, doi:10.1002/joc.2254.

Miguez-Macho, G., G. L. Stenchikov, and A. Robock, 2005: Regional climate simulations over North America: Interaction of local processes with improved large-scale flow. *J. Climate,* **18,** 1227–1246, doi:10.1175/JCLI3369.1.

Müller, O. V., E. H. Berbery, D. Alcaraz-Segura, and M. Ek, 2014: Regional model simulations of the 2008 drought in southern South America using a consistent set of land surface properties. *J. Climate,* **27,** 6754–6778, doi:10.1175/JCLI-D-13-00463.1.

Nogués-Paegle, J., and Coauthors, 2002: Progress in Pan American CLIVAR research: Understanding the South American monsoon. *Meteorologica,* **27,** 3–32.

Pohl, B., and J. Crétat, 2014: On the use of nudging techniques for regional climate modeling: Application for tropical convection. *Climate Dyn.,* **43,** 1693–1714, doi:10.1007/s00382-013-1994-3.

Radu, R., M. Déqué, and S. Somot, 2008: Spectral nudging in a spectral regional climate model. *Tellus,* **60A,** 898–910, doi:10.1111/j.1600-0870.2008.00341.x.

Roads, J., and A. Betts, 2000: NCEP–NCAR and ECMWF reanalysis surface water and energy budgets for the Mississippi River basin. *J. Hydrometeor.,* **1,** 88–94, doi:10.1175/1525-7541(2000)001<0088:NNAERS>2.0.CO;2.

Rodell, M., P. R. Houser, A. A. Berg, and J. S. Famiglietti, 2005: Evaluation of 10 methods for initializing a land surface model. *J. Hydrometeor.,* **6,** 146–155, doi:10.1175/JHM414.1.

Ruscica, R. C., A. A. Sörensson, and C. G. Menéndez, 2014: Hydrological links in southeastern South America: Soil moisture memory and coupling within a hot spot. *Int. J. Climatol.,* **34,** 3641–3653, doi:10.1002/joc.3930.

Schaake, J. C., V. I. Koren, Q.-Y. Duan, K. Mitchell, and F. Chen, 1996: Simple water balance model for estimating runoff at different spatial and temporal scales. *J. Geophys. Res.,* **101,** 7461–7475, doi:10.1029/95JD02892.

Seneviratne, S. I., T. Corti, E. L. Davin, M. Hirschi, E. B. Jaeger, I. Lehner, B. Orlowsky, and A. J. Teuling, 2010: Investigating soil moisture–climate interactions in a changing climate: A review. *Earth-Sci. Rev.,* **99,** 125–161, doi:10.1016/j.earscirev.2010.02.004.

Seth, A., and F. Giorgi, 1998: The effects of domain choice on summer precipitation simulation and sensitivity in a regional climate model. *J. Climate,* **11,** 2698–2712, doi:10.1175/1520-0442(1998)011<2698:TEODCO>2.0.CO;2.

Sörensson, A. A., and C. G. Menéndez, 2011: Summer soil–precipitation coupling in South America. *Tellus,* **63A,** 56–68, doi:10.1111/j.1600-0870.2010.00468.x.

——, ——, P. Samuelsson, and U. Hansson, 2010: Soil–precipitation feedbacks during the South American monsoon as simulated by a regional climate model. *Climatic Change,* **98,** 429–447, doi:10.1007/s10584-009-9740-x.

Trier, S., F. Chen, K. Manning, M. A. LeMone, and C. Davis, 2008: Sensitivity of the simulated PBL and precipitation to land surface conditions for a 12-day warm-season convection period in the central United States. *Mon. Wea. Rev.,* **136,** 2321–2343, doi:10.1175/2007MWR2289.1.

Wang, G., Y. Kim, and D. Wang, 2007: Quantifying the strength of soil moisture–precipitation coupling and its sensitivity to changes in surface water budget. *J. Hydrometeor.,* **8,** 551–570, doi:10.1175/JHM573.1.

Wei, J., and P. A. Dirmeyer, 2012: Dissecting soil moisture–precipitation coupling. *Geophys. Res. Lett.,* **39,** L19711, doi:10.1029/2012GL053038.

——, ——, and Z. Guo, 2010: How much do different land models matter for climate simulation? Part II: A decomposed view of the land–atmosphere coupling strength. *J. Climate,* **23,** 3135–3145, doi:10.1175/2010JCLI3178.1.

Yang, Z.-L., R. E. Dickinson, A. Henderson-Sellers, and A. J. Pitman, 1995: Preliminary study of spin-up processes in land surface models with the first stage data of Project for Intercomparison of Land Surface Parameterization Schemes Phase 1(a). *J. Geophys. Res.,* **100,** 16 553–16 578, doi:10.1029/95JD01076.

Zhang, J., W.-C. Wang, and L. R. Leung, 2008: Contribution of land–atmosphere coupling to summer climate variability over the contiguous United States. *J. Geophys. Res.,* **113,** D22109, doi:10.1029/2008JD010136.

Zhang, L., P. A. Dirmeyer, J. Wei, Z. Guo, and C.-H. Lu, 2011: Land–atmosphere coupling strength in the Global Forecast System. *J. Hydrometeor.,* **12,** 147–156, doi:10.1175/2010JHM1319.1.

Zhou, J., and K. M. Lau, 1998: Does a monsoon climate exist over South America? *J. Climate,* **11,** 1020–1040, doi:10.1175/1520-0442(1998)011<1020:DAMCEO>2.0.CO;2.